JOURNAL OF THERMOPHYSICS AND HEAT TRANSFER
Vol. 11, No. 4, October–December 1997

Steady-State Performance of a Rotating Miniature Heat Pipe

Lanchao Lin*
Wright State University, Dayton, Ohio 45435
and
Amir Faghri†
University of Connecticut, Storrs, Connecticut 06269-3139

The operating principle of a rotating miniature heat pipe (RMHP) with a grooved inner wall surface is addressed. A mathematical model of the hydrodynamic performance of RMHPs is developed. A simple correlation for the friction coefficient of axial liquid flow including a vapor drag effect is proposed, based on the numerical analysis of two-dimensional laminar liquid flow in a groove. With the present model, the maximum performance and optimum liquid fill amount of RMHPs are predicted under various operating conditions. Influences of operating temperature, rotational speed, and liquid–vapor interfacial shear stress on the maximum performance and optimum liquid fill amount are discussed. Pressure drops of the axial liquid flow and vapor flow are demonstrated.

Nomenclature

A = cross-sectional area, m^2
a_1, a_2 = constants
D_h = hydraulic diameter, m
Fr = Froude number, $\omega^2 s_b/g$
f = friction coefficient
g = gravitational acceleration, ms^{-2}
H_l = liquid depth, m
h_{fg} = latent heat of evaporation, J kg^{-1}
L = length, m
M = Mach number, $\bar{w}_{v,a}/\sqrt{\gamma_0 R_g T_v}$
M_t = total fluid mass, kg
N = rotational speed, rpm
N_g = number of grooves
P_v = wetted perimeter of vapor, m
p = pressure, N/m^2
Q = heat rate, W
Q_a = total heat input, W
q_c = heat flux of condensation, W m^{-2}
R = inner radius of a heat pipe, m
Re = vapor axial Reynolds number, $\rho_v D_{h,v} \bar{w}_v/\mu_v$
Re_l = liquid Reynolds number, $\rho_l D_{h,l} \bar{w}_l/\mu_l$
Re_r = vapor radial Reynolds number, $\rho_v D_{h,v} \bar{v}_{v,w}/\mu_v$
R_g = individual gas constant, J kg^{-1} K^{-1}
R_m = radius of curvature of the meniscus, m
s_a, s_b, s_t = radii, m
T_v = vapor temperature, °C
u = velocity in the x direction, ms^{-1}
v = radial velocity, ms^{-1}
w = axial velocity, ms^{-1}
$\bar{w}$ = mean axial velocity, ms^{-1}
x = coordinates, m
x_1 = half-side length of polygonal wall, m
y = coordinates, m
z = axial coordinate, m
β = momentum flux coefficient
γ = half-angle of the groove
γ_0 = ratio of specific heats
Δp = relative pressure, $p - p_{l0}$, N/m^2
δ = liquid film thickness, m
θ = meniscus contact angle
λ_1 = liquid–wall interface
λ_2 = liquid–vapor interface
μ = dynamic viscosity, Ns/m^2
ρ = mass density, kg m^{-3}
σ = surface tension, N/m
τ_v = interfacial shear stress, N/m^2
τ_v^* = dimensionless interfacial shear stress, $\tau_v/\rho_l \bar{w}_l^2$
ω = angular velocity, rad^{-1}

Subscripts
a = adiabatic
c = condenser
e = evaporator
l = liquid
max = maximum
op = optimum
t = total
v = vapor
w = wall
0 = evaporator end cap

Introduction

SINCE the concept of rotating heat pipes was proposed by Gray,[1] rotating heat pipes have found many applications in rotating components. One of the most successful applications for rotating heat pipes is in cooling electric motors and generators, allowing modern electric machines to have large loadings with a compact size. Marto[2] and Faghri[3] have given the overview of rotating heat pipe research and development. Most of the available research has taken motor cooling as a typical application background, where inner diameters of rotating heat pipes are larger than 10 mm, and the Froude number of rotating heat pipes is much larger than 1, that is, $Fr = \omega^2 R/g >> 1$. Little investigation has been reported, relating to the case of small diameter rotating heat pipes; although the corresponding application, such as drill bit cooling with a rotating heat pipe, has been proposed by Gray.[4]

To start the investigation of a rotating heat pipe having a small i.d. and operating horizontally, it is suggested that a series of triangular grooves be made along the heat pipe inner wall to use the resultant capillary pumping force as well as the centrifugal force to return the condensate to the evaporator

Received Nov. 21, 1996; revision received March 24, 1997; accepted for publication April 4, 1997.

*Research Associate, Department of Mechanical and Materials Engineering. Student Member AIAA.

†Professor and Head, Department of Mechanical Engineering. Associate Fellow AIAA.

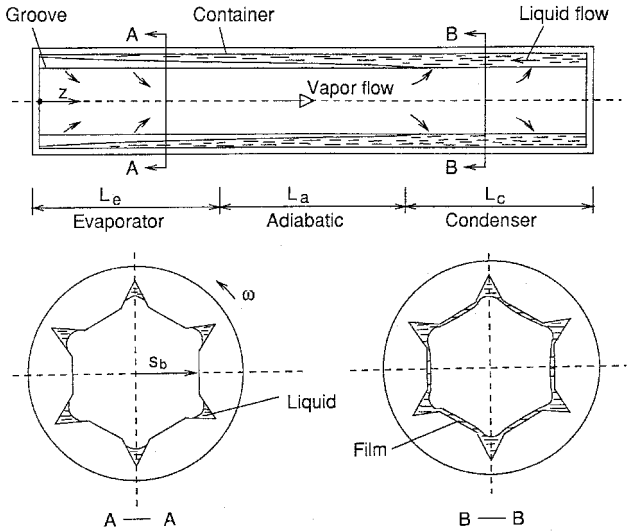

Fig. 1 Performance of an axially rotating miniature heat pipe with a polygonal inner wall with triangular grooves.

(Fig. 1). If the distance between a polygonal wall surface and the heat pipe centerline s_b is small and the rotational speed is not high, or $Fr < 1$, the capillary pumping force will become dominant in maintaining a steady two-phase flow circulation in the rotating heat pipe. In this case, the inner wall grooves serve not only as enhanced heat transfer surfaces, but, more significantly, as return liquid channels capable of pumping the condensate back to the evaporator. If the rotational speed is sufficiently high, i.e., $Fr >> 1$, the condensate return relies on the centrifugal force, and the grooves mainly improve the condensation heat transfer. We refer to this type of heat pipe as rotating miniature heat pipe (RMHP).

Since Cotter[5] introduced the concept of micro heat pipes for the cooling of electronic devices, numerous analytical and experimental investigations of micro and miniature heat pipes have been conducted. Detailed literature reviews related to micro and miniature heat pipes have been given by Cao and Faghri.[6] The rotating miniature heat pipe is expected to have many similar features of miniature heat pipes and rotating heat pipes with a relatively large i.d.. The object of the present study is to develop a mathematical model for prediction of the maximum performance and optimum liquid fill amount of RMHP. For modeling, a quasi-one-dimensional momentum equation of axial liquid flow and a simple formula for the friction coefficient of the axial liquid flow in triangular grooves are developed.

Operating Principles

As shown in Fig. 1, an axially rotating miniature heat pipe is horizontally oriented. It is composed of a series of triangular grooves machined along the inner wall to provide condensate return paths or liquid channels. In RMHPs, the thermal energy transport relies on the evaporation and condensation of a small amount of working fluid. The vaporization and condensation process causes the liquid–vapor interface in the liquid grooves to change continuously along the length. The change in the liquid–vapor interface has a twofold effect. A change in radius of curvature of the liquid–vapor interface causes a capillary pressure difference between the condenser and evaporator, which promotes the flow of condensate back to the evaporator. In addition, a varying liquid depth allows the centrifugal acceleration to produce a hydrostatic pressure change along the groove and, consequently, to pump the condensate back to the evaporator. In the condenser, the vapor condensates on the polygonal wall surface and forms a liquid film. The condensate of film flows circumferentially into the groove by the aid of the centrifugal force. Close to the evaporator end cap, the liquid meniscus is depressed in the groove corner, and its cross-sectional area and radius of curvature of the liquid–vapor interface are very small if the heat input is sufficiently high. The polygonal wall surface is dry in the evaporator. The counterflowing vapor exerts a shear force at the liquid free surface and decreases the maximum performance of the heat pipe. The maximum performance is believed to be reached if the capillary and centrifugal pumping forces are not sufficiently large to ensure a steady two-phase flow circulation in the heat pipe. Conceivably, to distribute most liquid in all grooves equally, the centrifugal force should be at least greater than the gravitational force, or the Froude number, defined as

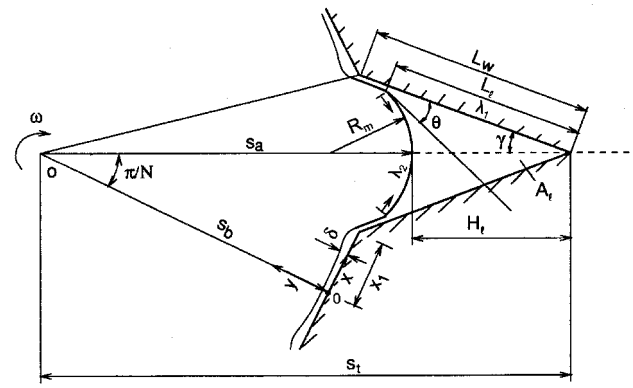

Fig. 2 Cross-sectional view of the rotating miniature heat pipe.

$$Fr = \omega^2 s_b / g \tag{1}$$

is greater than 1.

Steady-State Modeling

The fluid flow in a horizontally oriented RMHP is characterized by a circumferential liquid flow on the condensation surface of the polygonal wall surface, an axial liquid flow in the groove, and a countercurrent vapor flow with varied mass rate caused from evaporation and condensation. These flows are assumed to be one dimensional. Figure 2 shows a cross-sectional view of the heat pipe and liquid distribution in the condenser.

To obtain a high internal heat transfer coefficient and to prevent flooding of the countercurrent flow during operation of the RMHP, the liquid fill is controlled to ensure that no excess liquid blocks in the condenser end. In the modeling of hydrodynamic performance, the following assumptions are made:

1) The vapor and liquid flows are incompressible.
2) The liquid flow is laminar.
3) The radial heat flux applied at the evaporator is linearly decreased with the axial distance z, and the radial heat flux removed from the condenser is uniform.
4) The vapor and liquid are in the saturated state.
5) The effect of gravitational force on the flow is negligible.
6) Influences of the Coriolis force and surface tension on the circumferential condensate film flow are negligibly small.
7) The contact angle of the meniscus θ is constant.
8) A thin liquid film amount in the triangular groove region of $(L_w - L_l)$ is neglected.
9) The effect of vapor drag on the circumferential liquid film flow can be neglected.

At any axial location, the mass conservation over a cross section of the RMHP states

$$\bar{w}_v \rho_b A_v = N_g \bar{w}_l \rho_l A_l \tag{2}$$

where the cross-sectional areas of axial liquid flow and vapor flow are (see Fig. 2)

$$A_l = R_m^2\left[\cos(\gamma+\theta)\sin(\gamma+\theta)+\frac{\cos^2(\gamma+\theta)}{\tan\gamma}-\left(\frac{\pi}{2}-\gamma-\theta\right)\right] \tag{3}$$

$$A_v = N_g\left\{s_b^2\tan(\pi/N_g)+L_w\sin\gamma\left[s_t-\frac{s_b}{\cos(\pi/N_g)}\right]\right\}-N_gA_l \tag{4}$$

The distance between the heat pipe centerline and meniscus center point s_a (see Fig. 2) is given by

$$s_a = s_t - R_m\left[\frac{\cos(\gamma+\theta)}{\tan\gamma}-1+\sin(\gamma+\theta)\right] \tag{5}$$

Variations of A_v and A_l, with the length, depend on the variation of the liquid–vapor interfacial R_m, which is related to the pressure difference between the liquid and vapor by the Laplace–Young equation:

$$p_l = p_v - (\sigma/R_m) \tag{6}$$

Because there is no excess liquid accumulated in the end of condenser, M_t is calculated by

$$M_t = \int_{L_t}\rho_v A_v\,\mathrm{d}z + N_g\int_{L_t}\rho_l A_l\,\mathrm{d}z + 2N_g\rho_l L_c\int_{x_1}\delta\,\mathrm{d}x \tag{7}$$

where $L_t = L_e + L_a + L_c$.

Liquid Flow in a Groove

Since the effect of gravitational force on the flow is neglected, the liquid flow in the groove is independent of circumferential position. A momentum equation for the liquid flow in a stationary groove has been established[3] and, in the case of horizontal operation, can be expressed as

$$\frac{\mathrm{d}p_l}{\mathrm{d}z} = \mu_l\left(\frac{\partial^2 w_l}{\partial x^2}+\frac{\partial^2 w_l}{\partial y^2}\right) \tag{8}$$

In the present case of RMHP, a momentum equation can be formulated by introducing a centrifugal force term into Eq. (8) for the stationary heat pipe. The effect of centrifugal force is reflected by a varying H_l along the groove. A net driving pressure generated by the centrifugal force, acting on a control volume of the liquid flow in a groove, can be expressed as $\rho_l\omega^2 s_a\,\mathrm{d}H_l$, where H_l is shown in Fig. 2. The corresponding pressure gradient in the z direction is $\rho_l\omega^2 s_a\,\mathrm{d}H_l/\mathrm{d}z$, or $-\rho_l\omega^2 s_a\,\mathrm{d}s_a/\mathrm{d}z$. Adding this term of centrifugal force into Eq. (8), we obtain the momentum equation for the axial liquid flow in the rotating miniature heat pipe (nontapered), as follows:

$$\frac{\mathrm{d}p_l}{\mathrm{d}z}-\rho_l\omega^2 s_a\frac{\mathrm{d}s_a}{\mathrm{d}z} = \mu_l\left(\frac{\partial^2 w_l}{\partial x^2}+\frac{\partial^2 w_l}{\partial y^2}\right) \tag{9}$$

The term on the right-hand side (RHS) expresses the liquid viscous drag. If F refers to the left-hand part of Eq. (9), then Eq. (9) can be rewritten as

$$F = \mu_l\left(\frac{\partial^2 w_l}{\partial x^2}+\frac{\partial^2 w_l}{\partial y^2}\right) \tag{10}$$

As shown in Fig. 2, the liquid in the groove touches both walls, λ_1, and interacts with the vapor flow at the liquid–vapor interface, λ_2. The no-slip condition and relation for the quality of tangential shear stress on these surfaces are

$$w_l\big|_{\lambda_1} = 0, \qquad \mu_l\left.\frac{\partial w_l}{\partial n}\right|_{\lambda_2} = -\tau_v \tag{11}$$

where the liquid–vapor τ_v is given by

$$\tau_v = (f_v/2)\rho_v\bar{w}_v^2 \tag{12}$$

and n is the normal vector on the free surface of the liquid meniscus. To simulate the heating condition of a drill bit, a linear change in heat rate per unit axial length along the evaporator is assumed:

$$\frac{\mathrm{d}Q(z)}{\mathrm{d}z} = \frac{2Q_a}{L_e}\left(1-\frac{z}{L_e}\right) \tag{13}$$

In the condenser, the change is constant

$$\frac{\mathrm{d}Q(z)}{\mathrm{d}z} = -\frac{Q_a}{L_c} \tag{14}$$

Related to the changes in heat load, the energy equation can be cast into a form reflecting the change in the axial mass flow rate of liquid:

$$\frac{\mathrm{d}(\bar{w}_l\rho_l A_l)}{\mathrm{d}z} = \begin{cases}\dfrac{1}{Nh_{fg}}\dfrac{2Q_a}{L_e}\left(1-\dfrac{z}{L_e}\right) & 0\le z\le L_e\\ 0 & L_e < z\le L_e+L_a\\ -\dfrac{1}{Nh_{fg}}\dfrac{Q_a}{L_c} & L_e+L_a < z\le L_t\end{cases} \tag{15}$$

The axial liquid velocity at the evaporator end cap is zero:

$$\bar{w}_l\big|_{z=0} = 0 \tag{16}$$

The vapor and liquid pressures at the evaporator end cap are

$$p_v\big|_{z=0} = p_{v0}, \quad p_l\big|_{z=0} = p_{v0} - (\sigma/R_{m0}) \tag{17}$$

Given a value of F, Eq. (10), along with Eq. (11), describe a two-dimensional boundary value problem. To simplify the liquid momentum equation, a liquid friction coefficient f_l is defined by the following equation:

$$\mu_l\left(\frac{\partial^2 w_l}{\partial x^2}+\frac{\partial^2 w_l}{\partial y^2}\right) = f_l\frac{2\rho_l\bar{w}_l^2}{D_{h,l}} \tag{18}$$

which is subject to boundary condition (11), where $\bar{w}_l$ and $D_{h,l}$ are defined as

$$\bar{w}_l = \frac{1}{A_l}\int\int_{A_l} w_l(x,y)\,\mathrm{d}x\,\mathrm{d}y \tag{19}$$

$$D_{h,l} = \frac{4A_l}{2L_l} \tag{20}$$

and where

$$L_l = R_m\cos(\gamma+\theta)/\sin\gamma \tag{21}$$

Therefore, Eq. (10) can be replaced by a one-dimensional momentum equation with a liquid friction term on the RHS:

$$F = f_l \frac{2\rho_l \bar{w}_l^2}{D_{h,l}} \tag{22}$$

For a prescribed heat pipe geometry, a practical formula relating f_l to Re_l and a dimensionless liquid–vapor τ_v^* is supposed to have the following form:

$$f_l = \frac{a_1}{Re_l} + a_2 \tau_v^* \tag{23}$$

where Re_l and τ_v^* are defined as

$$Re_l = \frac{\rho_l \bar{w}_l D_{h,l}}{\mu_l} \tag{24}$$

$$\tau_v^* = \frac{\tau_v}{\rho_l \bar{w}_l^2} \tag{25}$$

The coefficients a_1 and a_2 in Eq. (23) are determined through regression of different data groups of f_l, Re_l, and τ_v^*, which result from solutions of the two-dimensional boundary-value problem, given by Eqs. (10) and (11), and Eqs. (19)–(22), (24), and (25), for various values of F and A_l.

Condensate Film

The coordinate system for condensate film flow is shown in Fig. 2. Under the assumption of negligible Coriolis force, the circumferential film flow is symmetrical about the rotational coordinate of y. Assuming that the condensate film thickness is very small compared to s_b, the momentum equations in the y and x directions for the condensate film flow and boundary conditions are similar to those used for rotating heat pipes with a large i.d.[7]

$$\frac{\partial p_l}{\partial y} + \rho_l \omega^2 (s_b - y) = 0 \tag{26}$$

$$-\frac{\partial p_l}{\partial x} + \rho_l \omega^2 x + \mu_l \frac{\partial^2 u_l}{\partial y^2} = 0 \tag{27}$$

subject to

$$y = 0, \qquad u_l = 0 \tag{28}$$

$$y = \delta, \qquad \frac{\partial u_l}{\partial y} = 0, \qquad p_l = p_v \tag{29}$$

$$x = 0, \qquad \frac{d\delta}{dx} = 0 \tag{30}$$

To close the solution of Eqs. (26) and (27), a boundary condition at $x = x_1$ is required. On the assumption that the liquid flow in the groove has no influence on the condensate film flow on the polygonal wall surface, this boundary condition is approximately written as

$$x = x_1, \qquad \frac{d\delta}{dx} = 0 \tag{31}$$

The energy equation can be expressed as

$$\frac{q_c x}{h_{fg}} = \int_0^\delta \rho_l u_l \, dy \tag{32}$$

where q_c is given by

$$q_c = Q_a / 2NL_c x_1 \tag{33}$$

Through mathematical treatments of the partial differential equations, (26) and (27), along with conditions (28) and (29), an ordinary differential equation (ODE) subject to condition (31) is reduced as follows:

$$(s_b - \delta) \frac{d\delta}{dx} = x \left(1 - \frac{3\mu_l q_c}{\rho_l^2 \omega^2 h_{fg} \delta^3} \right) \tag{34}$$

Boundary condition (30) is naturally satisfied.

Vapor Flow

The conservation of momentum equation for one-dimensional vapor flow is

$$\frac{dp_v}{dz} + \rho_v \frac{d}{dz} (\beta_v \bar{w}_v^2) = -f_v \frac{2\rho_v \bar{w}_v^2}{D_{h,v}} \tag{35}$$

where β_v, f_v, and $D_{h,v}$ are the momentum flux coefficient, the friction coefficient, and the hydraulic diameter of the vapor channel, respectively. $D_{h,v}$ is defined as

$$D_{h,v} = 4A_v / P_v \tag{36}$$

where P_v is approximately given by

$$P_v = 2N_g [x_1 + L_w - L_l + R_m[(\pi/2) - \theta - \gamma]] \tag{37}$$

The friction coefficient and momentum flux coefficient in the evaporator and adiabatic sections are calculated using the approximation of Khrustalev and Faghri,[8] based on the results given by Bankston and Smith[9]:

$$f_v = (16 + 0.46 Re_r - 0.017 Re_r^2)/Re, \quad \beta_v = 1.33 - 0.005 Re_r \tag{38}$$

where the radial Reynolds number and axial Reynolds number of vapor are defined, respectively, as

$$Re_r = \frac{\bar{v}_{v,w} D_{h,v} \rho_v}{\mu_v} \tag{39}$$

$$Re = \frac{\bar{w}_v D_{h,v} \rho_v}{\mu_v} \tag{40}$$

Equation (38) is applicable in the range of radial Reynolds numbers of $0 \leq Re_r < 20$. In the condenser section[10,11]

$$f_v = 16[1.2337 - 0.2337 \exp(-0.0363 Re_r)][\exp(1.2M)]/Re$$
$$\beta_v = 1.33 \tag{41}$$

Numerical Simulation

The first step is to determine the coefficients a_1 and a_2 in Eq. (23). The two-dimensional boundary-value problem, given by Eqs. (10) and (11), is solved for various values of F and a cross-sectional area of A_l using a finite element analysis methodology. In the analysis, triangular three-node elements are used, and meshes are generated on different cross-sectional areas of A_l. The side length of L_l, as shown in Fig. 2, is varied from 0.2 to 0.65 mm. The program output gives distributions of axial liquid velocity $w_l(x, y)$. The mean axial liquid velocity is then calculated using Eq. (19). From Eqs. (20)–(22), (24), and (25), the corresponding values of f_l, Re_l, and τ_v^* are further obtained, and they are used for regression of the coefficients a_1 and a_2, based on Eq. (23). As a result, we obtain the coefficients $a_1 = 13.163$ and $a_2 = 0.6211$. Intervals with 90% confidence are 13.123–3.203 for a_1 and 0.5938–0.6484 for

a_2. The correlation for the liquid friction coefficient for $\gamma = 20$ deg and $\theta = 30$ deg is therefore expressed as follows:

$$f_l = \frac{13.163}{Re_l} + 0.6211\tau_v^* \tag{42}$$

Errors of the prediction from Eq. (42) are between −2.8 and 1.3% of the result from the finite element analysis in the following ranges of parameter variation: $H_l = 0.2$–0.65 mm, $Q_a = 0.031$–24.0 W, $T_v = 110$°C, and $\tau_v = 7.7 \times 10^{-5}$–$0.055$ N/m^2. The next step is to solve ODEs (15), (22), and (35) in the z direction, as well as Eq. (34) in the x direction. The solution of Eq. (15), subject to Eq. (16), gives

$$\bar{w}_l \rho_l A_l = \begin{cases} \dfrac{2Q_a}{Nh_{fg}} \dfrac{z}{L_e}\left(1 - \dfrac{z}{2L_e}\right) & 0 \le z \le L_e \\ \dfrac{Q_a}{Nh_{fg}} & L_e < z \le L_e + L_a \\ \dfrac{Q_a}{Nh_{fg}} \dfrac{L_t - z}{L_c} & L_e + L_a < z \le L_t \end{cases} \tag{43}$$

Differentiating Eq. (6), and rearranging Eqs. (22) and (35), gives

$$\frac{dR_m}{dz} = \frac{R_m^2}{\sigma}\left(\frac{dp_l}{dz} - \frac{dp_v}{dz}\right) \tag{44}$$

$$\frac{dp_v}{dz} = -f_v \frac{2N^2 \rho_l^2 A_l^2 \bar{w}_l^2}{\rho_v D_{h,v} A_v^2} - \frac{d}{dz}\left(\frac{\beta_v N^2 \rho_l^2 A_l^2 \bar{w}_l^2}{\rho_v A_v^2}\right) \tag{45}$$

$$\frac{dp_l}{dz} = -\rho_l \omega^2 s_a \frac{s_t - s_a}{R_m} \frac{dR_m}{dz} + f_l \frac{2\rho_l \bar{w}_l^2}{D_{h,l}} \tag{46}$$

It is noted that since A_v and β_v change only slightly with length, the second term in Eq. (35), reflecting the dynamic change of the vapor flow, is approximately replaced by the second term on the RHS of Eq. (45). The boundary conditions corresponding to Eqs. (44)–(46), at $z = 0$, are

$$R_m = R_{m0}, \qquad p_v = p_{v0}, \qquad p_l = p_{v0} - (\sigma/R_{m0}) \tag{47}$$

where R_{m0} is related to the liquid fill amount at a given heat input. The system of ODEs (44)–(46) are solved numerically using the Runge–Kutta procedure. The controlled relative error is less than 10^{-5} for each of the variables. In solution, Eqs. (3)–(5), (20), (21), (24), (25), (36)–(41), (42), and (43) are also used. As a result, distributions of R_m, p_v, and p_l along the heat pipe can be obtained. The solution of Eq. (34), using the Runge–Kutta procedure, gives a liquid film thickness distribution in the x direction. The axial distributions of A_l and A_v are obtained using Eqs. (3) and (4). The liquid fill amount is then predicted by Eq. (7). The optimum liquid fill amount is such a value with which the maximum performance limitation is reached. At the maximum performance, the liquid at the condenser end cap ($z = L_t$) satisfies $L_l = L_w$, and R_{m0} has the smallest value possible, provided that Eqs. (44)–(46) can still be solved successfully. Close to the maximum performance, the variation of the heat rate with a decrease of R_{m0} is very small. The similar feature in a miniature heat pipe has been noted by Khrustalev and Faghri.[8] Therefore, the maximum performance can be found in the following way. Given a small value of R_{m0} and a value of Q_a, Eqs. (44)–(46) are solved, and a value of L_l at $z = L_t$ is obtained from Eq. (21). If $L_l < L_w$, the value of the total heat rate is increased by ΔQ_a. Repeat this procedure until the condition of $L_l|_{z=L_t} = L_w$ is satisfied. The heat rate corresponding to this case is the maximum performance Q_{max}.

Results and Discussion

For the numerical simulation, water is chosen as the working fluid. The heat pipe wall material is copper. The operating temperature, referring to the vapor temperature at the evaporator end cap, ranges from 80 to 140°C. The minimum θ is 33° for copper–water.[8] Dimensions of the polygonal heat pipe are as follows: $s_b = 1.3$ mm, $s_t = 2.0$ mm, $\gamma = 20$ deg, $L_w = 0.6724$ mm, $x_1 = 0.485$ mm, $L_e = 50$ mm, $L_a = 40$ mm, and $L_c = 50$ mm.

Figure 3 shows the predicted maximum performance as a function of the rotational speed at three different operating temperatures, 140, 110, and 90°C. The maximum performance increases with an increase of rotational speed and operating temperature. At $T_v = 110$°C, Q_{max} can be increased by 14.5%, if the rotational speed is increased from 1200 to 2400 rpm. At $N = 1200$ rpm ($Fr = 2.63$), Q_{max} is enhanced by 21% if the operating temperature rises from 90 to 110°C. The influence of the liquid–vapor interfacial shear stress on Q_{max} is shown in Fig. 4. The maximum performance of RMHP, including the vapor drag effect, is significantly lower than that neglecting this effect. The influence of the interfacial shear stress is more evident at low operating temperatures than at high operating temperatures. At $T_v = 80$°C, the Q_{max} with interfacial shear stress is 30% higher than that of no interfacial shear stress effect. Figure 5 shows variations of the relative pressures of $p_l - p_{l0}$ and $p_v - p_{l0}$ with the heat pipe length. The pressure drop is much higher in the liquid than in the vapor at higher heat rates, $Q > 10.0$ W. As the heat rate approaches the maximum performance, the pressure drop of the axial liquid flow over the heat pipe length increases significantly. Most of the pressure drop appears in the region close to the evaporator end cap, $0 < z < 0.2$ m, since A_l becomes significantly small in this region. The pressure drop in the vapor increases slightly as Q_a

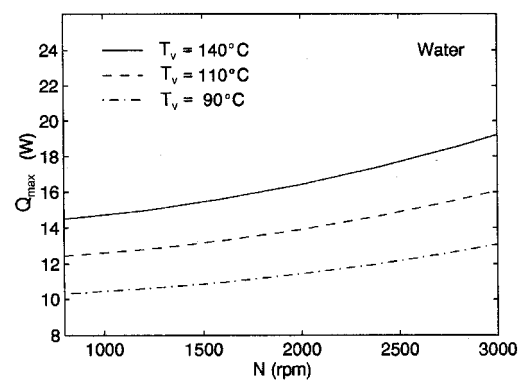

Fig. 3 Influences of the rotational speed and operating temperature on the maximum performance of the rotating miniature heat pipe.

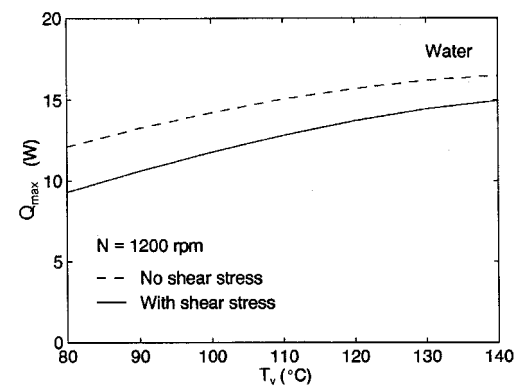

Fig. 4 Maximum performances of the rotating miniature heat pipe with and without shear stress at the liquid–vapor interface vs operating temperature.

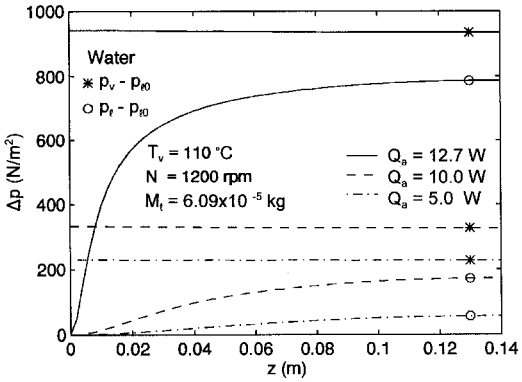

Fig. 5 Variations of the relative pressures of liquid and vapor along the length at different heat rates for a rotating miniature heat pipe.

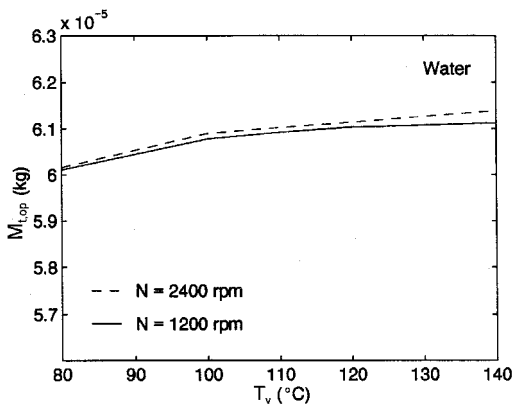

Fig. 6 Optimum liquid fill amount as a function of operating temperature for a rotating miniature heat pipe.

is close to the maximum performance (Q_{max} = 12.8 W). The optimum liquid fill amounts $M_{f,op}$, as a function of the operating temperature at N = 2400 and 1200 rpm, are presented in Fig. 6. The influence of the rotational speed on the optimum liquid fill amount is very small. The optimum liquid fill amount increases only slightly with an increase of operating temperature. It is a beneficial feature for the RMHP design that the optimum liquid fill amount of RMHP need not be changed if the operating temperature and rotational speed are varied.

Compared to the liquid amount in the grooves, the film liquid amount is a small fraction of $M_{f,op}$. At T_v = 110°C, N = 1200 rpm and Q_{max} = 12.8 W, for instance, the film liquid amount is 4.6% of $M_{f,op}$, whereas that in the grooves is 94.2%. As the rotational speed increases to N = 2400 rpm at T_v = 110°C and Q_{max} = 14.65 W, the film liquid amount is only 3.0% of $M_{f,op}$. The condensate film thickness δ is much smaller than s_b. For example, δ is only 1.1% of s_b at T_v = 140°C, N = 800 rpm, and Q_{max} = 14.5 W. It should be noted that under the present operating conditions, Re_r is smaller than 7.0.

It should be noted that the predicted maximum performance of RMHP under the condition of centrifugal force field is actually a capillary limitation. In numerical simulation, this limitation corresponds to the case where the solution of ODEs (44)–(46) begins to change dramatically with a slight increment of heat rate. The similar characteristic of the capillary limitation has been addressed in the analysis of performance limitation in a stationary micro heat pipe.[8]

To enhance the maximum performance of the modeled RMHP, the groove number can be increased to a certain extent, since the increase in the groove number can decrease the axial liquid flow resistance. The groove number also has an influence on the heat pipe internal heat transfer coefficient.

Conclusions

The hydrodynamic performance of a rotating miniature heat pipe is numerically simulated, based on the present mathematical model, and the results can be summarized as follows:

1) The maximum RMHP performance increases with an increase of the rotational speed and operating temperature.

2) The friction coefficient of liquid flow in a groove can be correlated to the liquid Reynolds number and a dimensionless liquid–vapor interfacial shear stress by a simple formula, based on the results of numerical analysis.

3) The pressure drop of axial liquid flow over the heat pipe length increases significantly as the heat rate approaches the maximum performance. The liquid pressure drop in the region close to the evaporator end cap is much higher than that in the other regions of the heat pipe.

4) Influences of the operating temperature and rotational speed on the optimum liquid fill amount are very small.

References

[1]Gray, V. H., "The Rotational Heat Pipe—A Wickless Hollow Shaft for Transferring High Heat Fluxes," American Society of Mechanical Engineers, Paper 69-HT-19, 1969.

[2]Marto, P. J., "Rotating Heat Pipes," *XIV. ICHTM Symposium, Heat and Mass Transfer in Rotating Machinery* (Dubrovnik), 1982, pp. 609–632.

[3]Faghri, A., "Heat Pipe Science and Technology," Taylor and Francis, Washington, DC, 1995.

[4]Gray, V. H., "Method and Apparatus for Heat Transfer in Rotating Bodies," U.S. Patent, No. 3,842,596, 1974.

[5]Cotter, T. P., "Principles and Prospects for Micro Heat Pipes," *Proceedings of the 5th International Heat Pipe Conference* (Tsukuba, Japan), 1984, pp. 328–335.

[6]Cao, Y., and Faghri, A., "Micro/Miniature Heat Pipes and Operating Limitations," *Enhanced Heat Transfer*, Vol. 1, No. 3, 1994, pp. 265–274.

[7]Vasiliev, L. L., and Khrolenok, V. V., "Heat Transfer in Rotating Heat Pipes," *Proceedings of the 7th International Heat Pipe Conference* (Minsk), 1990, pp. 285–293.

[8]Khrustalev, D., and Faghri, A., "Thermal Analysis of a Micro Heat Pipe," *Journal of Heat Transfer*, Vol. 116, No. 1, 1994, pp. 189–198.

[9]Bankston, C. A., and Smith, H. I., "Vapor Flow in Cylindrical Heat Pipes," *Journal of Heat Transfer*, Vol. 95, 1973, pp. 371–376.

[10]Bowman, W. J., and Hitchcock, J. E., "Transient, Compressible Heat Pipe Vapor Dynamics," *Proceedings of the ASME National Heat Transfer Conference* (Houston, TX), Vol. 1, 1988, pp. 329–338.

[11]Jang, J. H., Faghri, A., and Chang, W. S., "Analysis of the Transient Compressible Vapor Flow in Heat Pipes," *International Journal of Heat and Mass Transfer*, Vol. 34, No. 8, 1991, pp. 2029–2037.